RSC Advances

PAPER

View Article Online
View Journal | View Issue

Cite this: *RSC Adv.*, 2025, **15**, 18490

Design, synthesis and cytotoxic research of a novel antitumor model based on acrylamide–PABA analogs *via* β-tubulin inhibition†

Maha Ali Alghamdi,[a] Mustafa R. Abdulbaqi,[b] Dalal Sulaiman Alshaya,[c] Jawaher Alharthi,[a] Hanadi A. Katouah,[d] Fahmy Gad Elsaid,[e] Eman Fayad,[a] Ali H. Abu Almaaty,*[f] Abdullah Yahya Abdullah Alzahrani[g] and Botros Y. Beshay[h]

Received 7th April 2025
Accepted 15th May 2025

DOI: 10.1039/d5ra02384j

rsc.li/rsc-advances

Currently, the human health is facing numerous challenges, especially with regard to cancer. Therefore, new treatment options that specifically target tumor cells will inevitably improve the therapeutic toolkit for various cancers. In this regard, a sequence of acrylamide–PABA hybrids **4a–j** was synthesized, and their formation was confirmed *via* spectral and elemental analyses. The compounds were evaluated for their antiproliferative activity against MCF-7 (breast), HepG2 (liver) and a normal health breast cell line (MCF-10A). Among the series, acrylamide–PABA analog **4j** with a furan group in the acrylamide moiety was the most potent anti-proliferative member with a notable IC_{50} value (IC_{50} = 1.83 μM) against MCF-7 cells. Compound **4j**'s anti-tubulin activity and apoptosis-promoting properties were the cause of its anti-proliferative inhibitory mechanism. Compound **4j** promoted apoptosis in MCF-7 cells by raising the expression of apoptotic markers, such as p53, Bax, Bcl-2 and caspase 9, with respect to the untreated control. The molecular docking study of compound **4j** revealed a nice fitting into the active site of tubulin.

1. Introduction

Breast cancer represents the most commonly diagnosed lethal malignancy, and it is the leading cause of cancer-related deaths in women worldwide, presenting a critical global health issue.[1,2] It is experienced by millions each year and is the most common cancer type occurring among women, and the second most common cancer type overall.[3] In 2022, an estimated 2.3 million new cases and 670 000 deaths related to this disease was reported. The incidence rate is still increasing (1–5% per year).[4,5] Hence, ongoing research focuses on unravelling the molecular mechanisms driving breast cancer to advance approaches toward its prevention, early detection, and therapeutic strategies.[6,7]

Tubulin is a dominant structural protein that is essential for the formation of microtubules, which are essential targets in breast cancer. Microtubule-targeting agents (MTAs), like taxanes (*e.g.*, paclitaxel and docetaxel) are commonly used to treat various breast cancers, including triple-negative breast cancer (TNBC).[8–10] These drugs disrupt microtubule dynamics, stop cell division and trigger apoptosis. However, resistance to the existing MTAs has spurred the development of new tubulin inhibitors that target complementary binding sites, such as the colchicine-binding site, to inhibit microtubule polymerisation.[11–13]

Building on these findings, we aimed at designing potential tubulin inhibitors using a hybrid structure-based approach, focusing on acrylamide–PABA–combretastatin analogues as promising candidates. The anticancer activity of the acrylate moiety proceeds through a combined mechanism that includes β-tubulin and protein kinase inhibition.[14–16] Moreover, with a strong antimitotic effect, CA-4 (Combretastatin A-4) binds to the colchicine site. A better binding affinity is also shown by the dimethoxybenzene moiety and other parts. CA-4 has advanced to phase II and III clinical studies.[17,18] However, its clinical utility is limited by its pharmacokinetic parameters like low aqueous solubility, short plasma half-life, and isomerization from active *cis* to inactive trans under physiological settings.[19,20]

[a]*Department of Biotechnology, College of Sciences, Taif University, P.O. Box 11099, Taif 21944, Saudi Arabia*

[b]*Department of Pharmaceutics, College of Pharmacy, Al-Naji University, Baghdad 10015, Iraq*

[c]*Department of Biology, College of Science, Princess Nourah bint Abdulrahman University, P.O. Box 84428, Riyadh 11671, Saudi Arabia*

[d]*Chemistry Department, College of Science, Umm Al-Qura University, 21955, Makkah, Saudi Arabia*

[e]*Department of Biology, College of Science, King Khalid University, PO Box 960, Asir, Abha, 61421, Saudi Arabia*

[f]*Department of Zoology, Faculty of Science, Port Said University, Port Said, Egypt. E-mail: aliabuelmaaty8@gmail.com*

[g]*Department of Chemistry, Faculty of Science, King Khalid University, Abha 61413, Saudi Arabia*

[h]*Pharmaceutical Sciences (Pharmaceutical Chemistry) Department, College of Pharmacy, Arab Academy for Science, Technology and Maritime Transport, Alexandria P.O. Box 1029, Egypt*

† Electronic supplementary information (ESI) available. See DOI: https://doi.org/10.1039/d5ra02384j

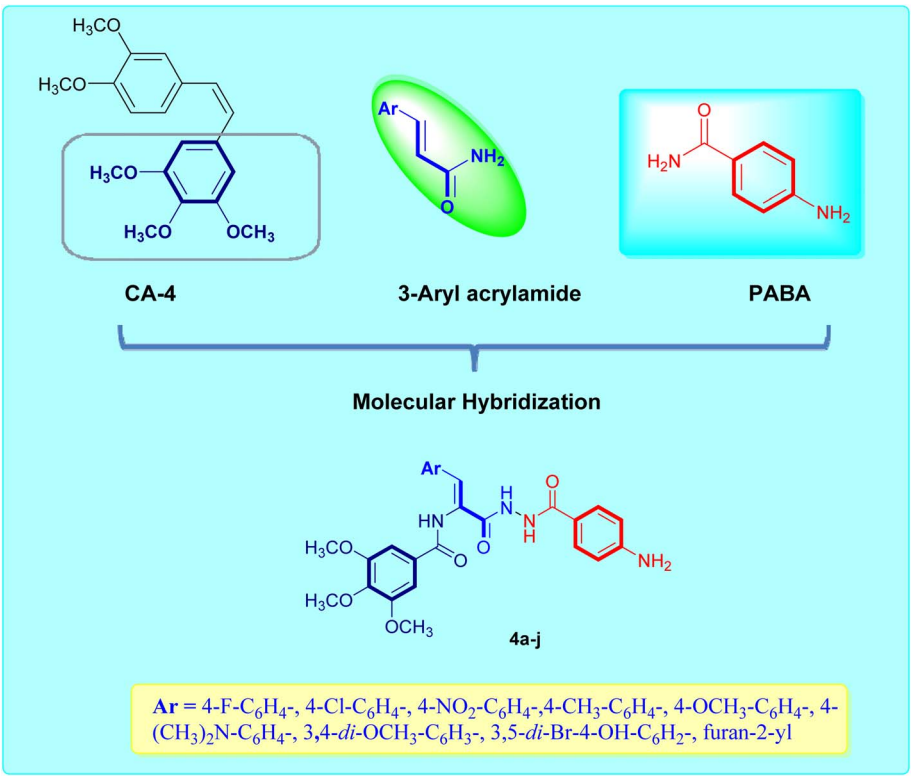

Fig. 1 Molecular design of the target acrylamide–PABA–CA-4 hybrids.

The current study attempts to overcome the poor pharmacokinetics of CA-4 and growing resistance to the available cancer therapies through a new building block, namely, *p*-aminobenzoic acid (PABA). PABA is recognised for its structural diversity at the amino and carboxyl groups and can act as an outstanding building block. PABA-based hybrid compounds exhibit antioxidant, anti-inflammatory, anticancer and antimicrobial potential in clinical applications.[21,22] PABA derivatives also have been demonstrated to have various modes of action in cancer chemotherapy, including the inhibition of β-tubulin and protein kinases, further supporting their potential as therapeutic agents.[23,24] In this work, we integrated *p*-aminobenzoic acid (PABA), the acrylate platform and trimethoxybenzene moiety from CA-4 (Fig. 1) into a single molecular entity to enhance its pharmacokinetic profile, along with improved inhibition of microtubule polymerization. We have also introduced several substitution patterns on the aryl group linked to the acrylamide part to assess their impact on tubulin binding and inhibitory activity akin to colchicine. This design strategy will assess the antiproliferative potential of the newly synthesized compounds against the MCF-7 breast cancer cell line.

2. Results and discussion

2.1. Chemistry

The synthetic employed pathway to prepare the new acrylamide–PABA analogs **4a–j** is outlined in Scheme 1. The chemical synthesis was initiated by heating 4-aminobenzoic acid (**1**) with pure ethanol in the presence of concentrated sulphuric acid at reflux temperature to furnish ethyl 4-aminobenzoate (**2**). The obtained ester **2**, on heating to reflux with hydrazine hydrate in pure ethanol, gave 4-aminobenzoic acid hydrazide (**3**) in good yield. The target acrylamide–PABA analogs **4a–j** were prepared by reaction of the key hydrazide intermediate **3** with the appropriate ethyl 3-arylacrylate molecule in refluxing pure ethanol using a catalytic amount of glacial acetic acid to yield the desired acrylamide–PABA products **4a–j**. The formation of the desired acrylamide–PABA products **4a–j** was evidenced by spectral data (^{1}H-NMR and ^{13}C-NMR spectra), in addition to elemental analysis.

As a representative example of these series, the ^{1}H-NMR spectrum of **4j** showed the presence of three singlet signals at δ_H 10.01, 9.96 and 9.83 ppm, evidencing the presence of three NH amidic protons, and also the presence of two aromatic sets of C2,6-Hs and C3,5-Hs of the phenyl ring of the PABA moiety as doublet signals at δ_H 7.65 and 6.57 ppm, respectively, with J value = 8.2 Hz. In addition, there are two singlet signals with two-proton integration at δ_H 7.40 and 5.71 ppm attributed to the phenyl ring of the 3,4,5-trimethoxyphenol moiety and amino (NH_2) protons of the *p*-aminobenzoic acid moiety. The olefinic proton was also observed as a singlet signal at δ_H 7.24 ppm. Furthermore, the ^{1}H-NMR spectrum of the acrylamide–PABA analog **4j** displayed two singlet signals at 3.87 and 3.75 ppm for six- and three-protons integration, which correspond to the aliphatic methoxyls' of the 3,4,5-trimethoxyphenyl motif. ^{13}C-NMR spectrum of the acrylamide–PABA analog **4j** displayed three signals in the range of δ_C 166.06–164.68 ppm assigned to the amide carbonyl groups, and two characteristic aliphatic

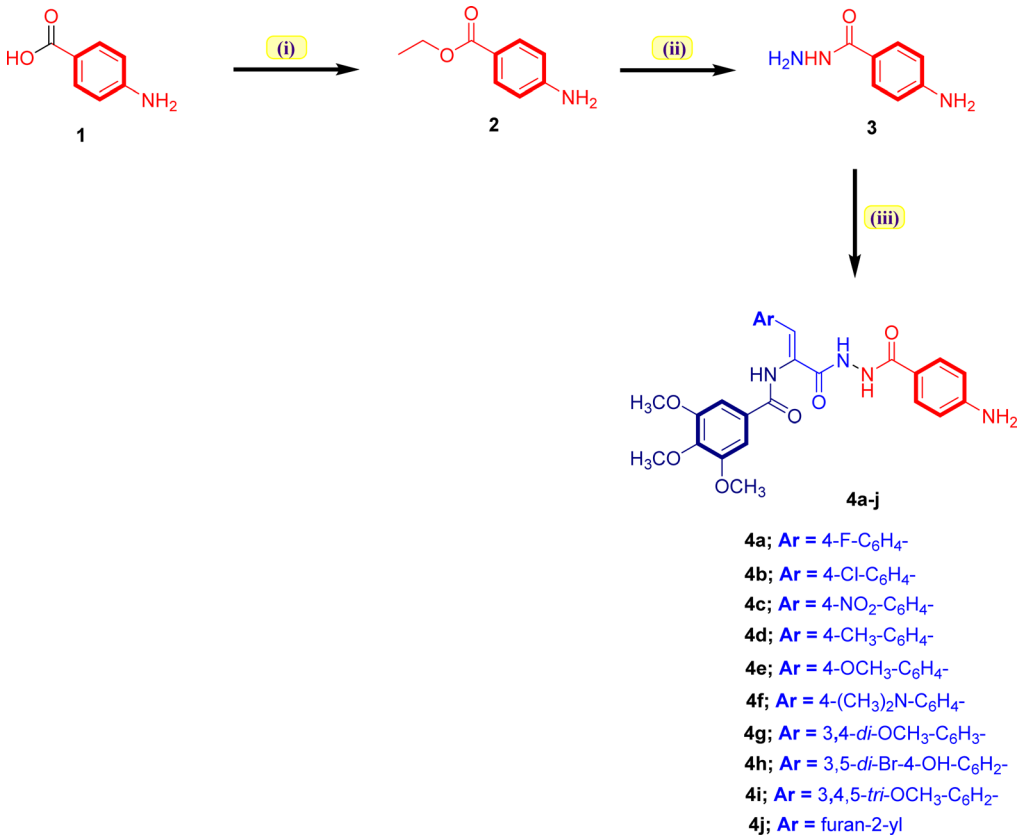

Scheme 1 Synthesis of the targeted 3-arylacrylamide–PABA analogs **4a–j**. Reaction conditions: (i) EtOH, conc. H_2SO_4, reflux 12 h; (ii) NH_2-$NH_2 \cdot H_2O$, EtOH, reflux 4 h; (iii) appropriate ethyl 3-arylacrylate, EtOH, AcOH, reflux 10–12 h.

signals with two- and one-carbon integration at δ_C 60.58 and 56.53 ppm, respectively, which were ascribed to the aliphatic methoxyls of the 3,4,5-trimethoxyphenyl group. In addition, the ^{13}C-NMR spectrum of the acrylamide–PABA analog **4j** demonstrated all other aromatic and olefinic carbons, which appeared at their expected chemical shifts. Finally, data from the elemental analysis further confirmed the assigned structure.

2.2. Biology

2.2.1. Cytotoxic activity of the acrylamide–PABA analogs against the MCF-7 cell line. The MTT colorimetric technique was used to evaluate the cytotoxic activity of the newly produced acrylamide–PABA hybrids **4a–j** against the MCF-7 breast cancer cell line. Colchicine (Col) was utilized as a reference cytotoxic agent in this assay technique. Table 1 shows the results as an IC_{50} for each test compound. In general, most of the examined analogs had good cytotoxic activity against MCF-7 cells with IC_{50} values ranging from 1.83–73.11 μM. Among these analogs, compounds **4c, 4d** and **4e** showed weak activity toward the MCF-7 cell line (IC_{50} > 30 μM) compared to Col (IC_{50} = 3.54 μM). The remaining analogs showed low micromolar IC_{50} values (IC_{50} < 30 μM). In particular, compounds **4a** and **4j** displayed the most activity of the new compounds with IC_{50} values of 2.99 and 1.83 μM, respectively. The structure activity relationship (SAR) analysis of the aryl ring-attached acrylamide moiety indicated an influence on the antiproliferative activity. Introduction of an electron-withdrawing group such as the 4-fluorphenyl group in compound **4a** or the 4-chlorophenyl group in compound **4b** resulted in an increase in the antiproliferative activity with an IC_{50} value of 2.99 and 25.27 μM, respectively. However, increasing the number of electron-withdrawing substituents (such as compound **4h** with dibromo substituents) increased the antiproliferative activity (IC_{50} = 19.92 μM). Moreover, upon the introduction of electron-donating groups (such as the 4-methylphenyl group in compound **4d** or 4-methoxyphenyl in compound **4e**), the cytotoxic efficacy was notably decreased with an IC_{50} value of 73.11 and 64.61 μM, respectively. Furthermore, the introduction of a polysubstituted phenyl ring (such as 3,4-dimethoxyphenyl in compound **4g** and 3,4,5-trimethoxyphenyl in compound **4i**) led to a notable increase of the cytotoxic activity with an IC_{50} value of 17.10 and 4.51 μM, respectively. Again, the cytotoxic activity was significantly increased in acrylamide–PABA **4j** when the substituted phenyl ring was replaced with a heterocyclic moiety such as furan with an IC_{50} value of 1.83 μM, which was superior to Col (1.9-fold more potent than the reference drug). These results demonstrated the importance of the heterocyclic substitution in the acrylamide moiety and the activity increased in the following order: furan > polysubstituted phenyl ring > phenyl ring decorated with electron-withdrawing groups > phenyl ring having electron-donating substituents. In addition, the acrylamide–PABA compounds that demonstrated notable cytotoxic activity against

Table 1 *In vitro* cytotoxic evaluation of the constructed acrylamide–PABA analogs **4a–j** against MCF-7 breast carcinoma cells[a]

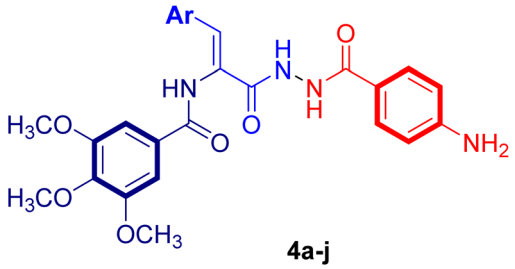

4a-j

Comp. no.	Ar	IC_{50} (μM) MCF-7	HepG2	MCF-10A
4a	4-F–C_6H_4–	2.99 ± 0.10	4.87 ± 0.13	19.76 ± 0.62
4b	4-Cl–C_6H_4–	25.27 ± 0.86	ND	ND
4c	4-NO_2–C_6H_4–	39.69 ± 1.34	ND	ND
4d	4-CH_3–C_6H_4–	73.11 ± 2.47	ND	ND
4e	4-OCH_3–C_6H_4–	64.61 ± 2.19	ND	ND
4f	4–$(CH_3)_2N$–C_6H_4–	27.22 ± 0.92	ND	ND
4g	3,4-di-OCH_3–C_6H_3–	17.10 ± 0.58	ND	ND
4h	3,5-di-Br-4-OH–C_6H_2–	19.92 ± 0.67	ND	ND
4i	3,4,5-tri-OCH_3–C_6H_2–	4.51 ± 0.15	ND	ND
4j	Furan-2-yl	1.83 ± 0.06	2.14 ± 0.09	23.21 ± 1.06
Col	—	3.54 ± 0.08	4.05 ± 0.07	27.54 ± 0.11

[a] All experiments were carried out in triplicate; ND, not determined.

MCF-7 cells were assessed further to determine their IC_{50} values against the HepG2 hepatocellular carcinoma cell line (Table 1). All examined compounds demonstrated better cytotoxic activity against HepG2 cells relative to the reference drug Col. Additionally, the MCF-10A (normal breast) cell line was used to assess the antiproliferative efficacy of the active acrylamide–PABA compounds **4a** and **4j** (Table 1). It is clear from the IC_{50} values that the examined active molecules showed less cytotoxicity against the normal breast cell line (MCF-10A) relative to the anticancer potential against the carcinoma cell lines, which supports the anticancer properties of the acrylamide–PABA compounds.

2.2.2. Acrylamide–PABA analogs 4a and 4j inhibited β-tubulin polymerization in MCF-7 cells. The process of the tubulin-microtubule polymerization of a cancer mass usually leads to aggressive tumor growth and metastasis.[25] This link between the abnormal tubulin assembly and tumor growth is strong owing to the excessive tubulin polymerization in more lethal cancer such as breast cancer.[26] Dual inhibitors of cancer cell proliferation and tubulin polymerization have recently shown their remarkable potential against several cancers.[27] The two most potent analogs **4a** and **4j** were next examined for their potency as β-tubulin inhibitors using the β-tubulin assay kit. Fig. 2 shows the data as the percentage inhibition for each analog using Col as a reference drug. The results indicated that the examined analogs **4a** and **4j** inhibited β-tubulin polymerization with a percentage inhibition of 78.19% and 81.51%, respectively, when compared to the reference Col (percentage inhibition of 84.33%). Compound **4j** (Ar = furan-2yl), the most potent antiproliferative agents, displayed the greatest inhibitory efficacy against β-tubulin polymerization with a percentage inhibition of 81.51%, which was comparable to Col. On the other hand, compound **4a** (Ar = 4-fluorophenyl) ranks second in β-tubulin polymerization inhibition activity with a percentage inhibition value of 78.19%. The results of this assay method indicated that acrylamide–PABA analogs **4a** and **4j** had substantial antiproliferative activity against MCF-7 and as potent β-tubulin inhibitors.

2.2.3. Acrylamide–PABA analog 4j induced cellular apoptosis in MCF-7 cells. Understanding the biological mechanism of action of chemotherapeutic agents is an important

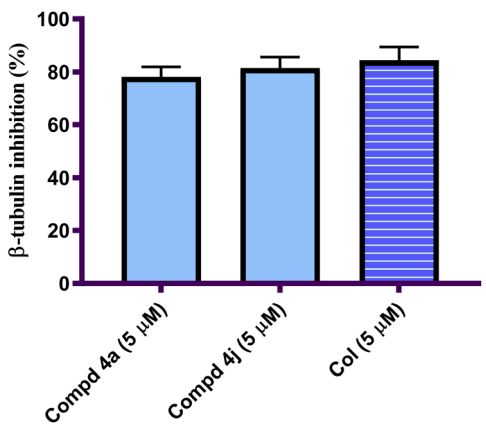

Fig. 2 Representation of the percentage of β-tubulin polymerization on MCF-7 cells stimulated by acrylamide–PABA analogs **4a** and **4j** relative to Col.

aspect of the pharmaceutical development process.[28] Recently, the activation of apoptosis through pharmacological manipulation of malignant cells' growth suppression and antiproliferative action has been demonstrated as a unique approach for chemotherapeutic detection and screening.[29] To better understand the pathway that allowed the produced analogs to elicit the cytotoxic action, we incubated the most active acrylamide–PABA **4j** with MCF-7 cells for 48 h. Following cellular staining with Annexin V –FITC/propidium iodide (PI), FACS analysis was conducted. To differentiate between early and late apoptosis, both stains were used. (PI^-/Annexin V-$FITC^+$) represented early apoptotic cells, (PI^+/Annexin V-$FITC^+$) indicated late apoptotic cells, and (PI^+/Annexin V-$FITC^-$) represented necrotic cells. However, healthy cells were not stained (PI^-/Annexin V-$FITC^-$). Fig. 3 shows the dot plot of the most active analog **4j**. As seen in Fig. 3, compound **4j** primarily used apoptosis to exhibit its cytotoxic activity. This was clarified by compound **4j**'s modest degree of induced necrosis in contrast to its markedly elevated levels of induced early and late apoptosis. Acrylamide–PABA analog **4j** induced both early apoptosis (22.07%) and late apoptosis (7.56%) in comparison with modest level of necrosis (3.19%). These data indicated that acrylamide–PABA analog **4j** demonstrated its cytotoxic effects mainly through apoptosis.

2.2.4. Acrylamide–PABA analog 4j enhanced the level of apoptotic markers in MCF-7 cells. The apoptotic markers related to apoptosis were crucial in preventing cancer.[30] p53 and other apoptotic regulators function as transcription factors that can activate several target genes in response to oncogenic stress, causing cell cycle arrest, apoptosis activation, and degeneration, while also promoting DNA repairs.[31] As a result, the apoptosis-related markers work together in order to ensure that cells with mutations that promote cancer (including broken genomes) are either repaired or permanently eliminated.[32] To further comprehend the molecular process involved in the apoptotic efficacy of the acrylamide–PABA analogs, the expression levels of p53, Bax, Bcl-2 and *c*aspase 9 were evaluated. These genes' expression levels were investigated in the presence of acrylamide–PABA analog **4j**, which demonstrated significant apoptotic activity. This was carried out in contrast to a negative control group. As illustrated in Fig. 4, the acrylamide–PABA **4j** analog displayed a significant elevation in the expression level of p53 (5.14-fold), Bax (8.36-fold) and *c*aspase 9 (9.89-fold) compared to the negative controls. This was accompanied by a notable drop in the level of Bcl-2 (0.29-fold). These data explained that the enhanced expression of the apoptotic markers is the main mechanism underlying the acrylamide–

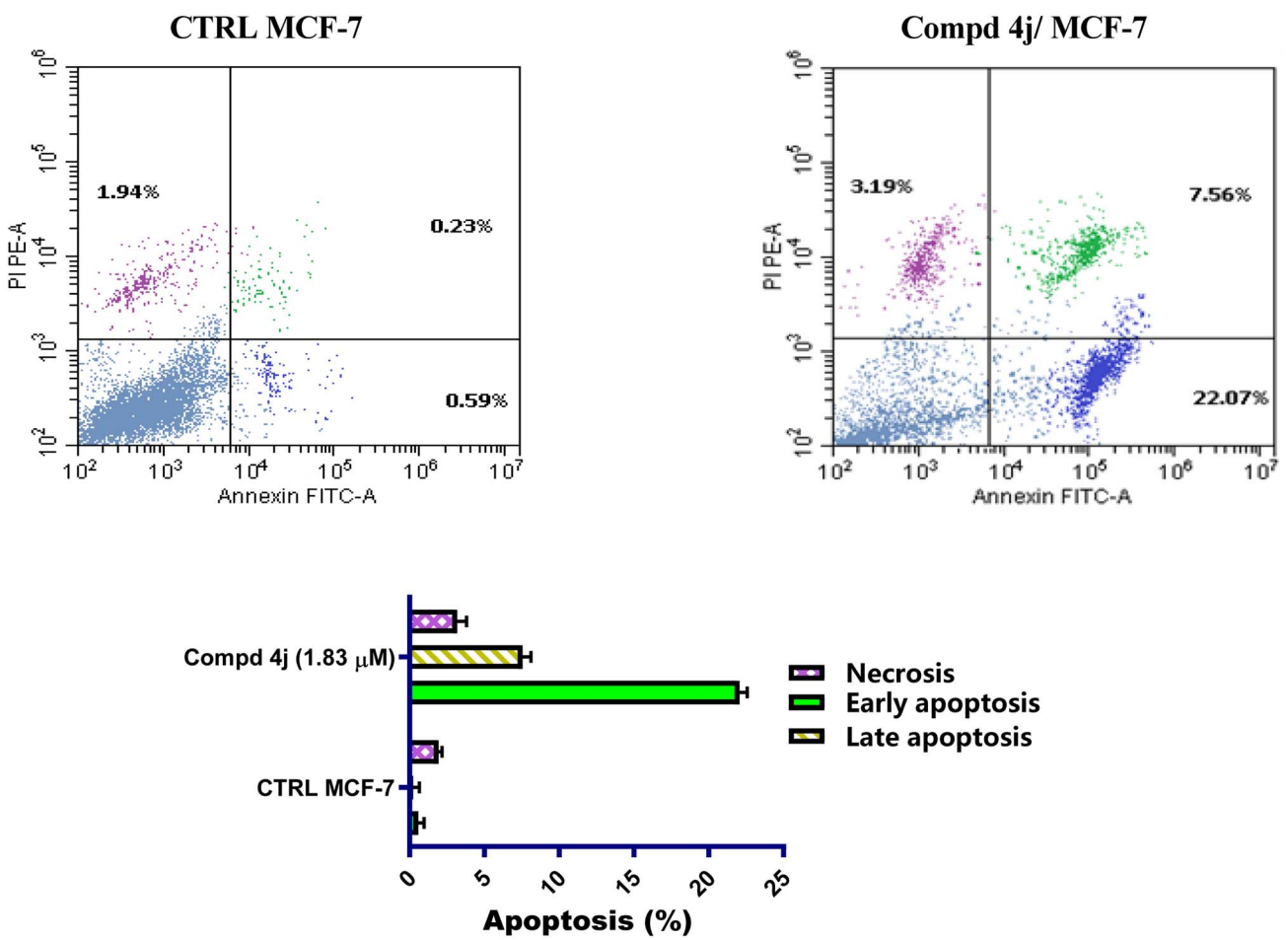

Fig. 3 Comparison between the apoptosis influence on MCF-7 cells stimulated by acrylamide–PABA analog **4j** and untreated control cells.

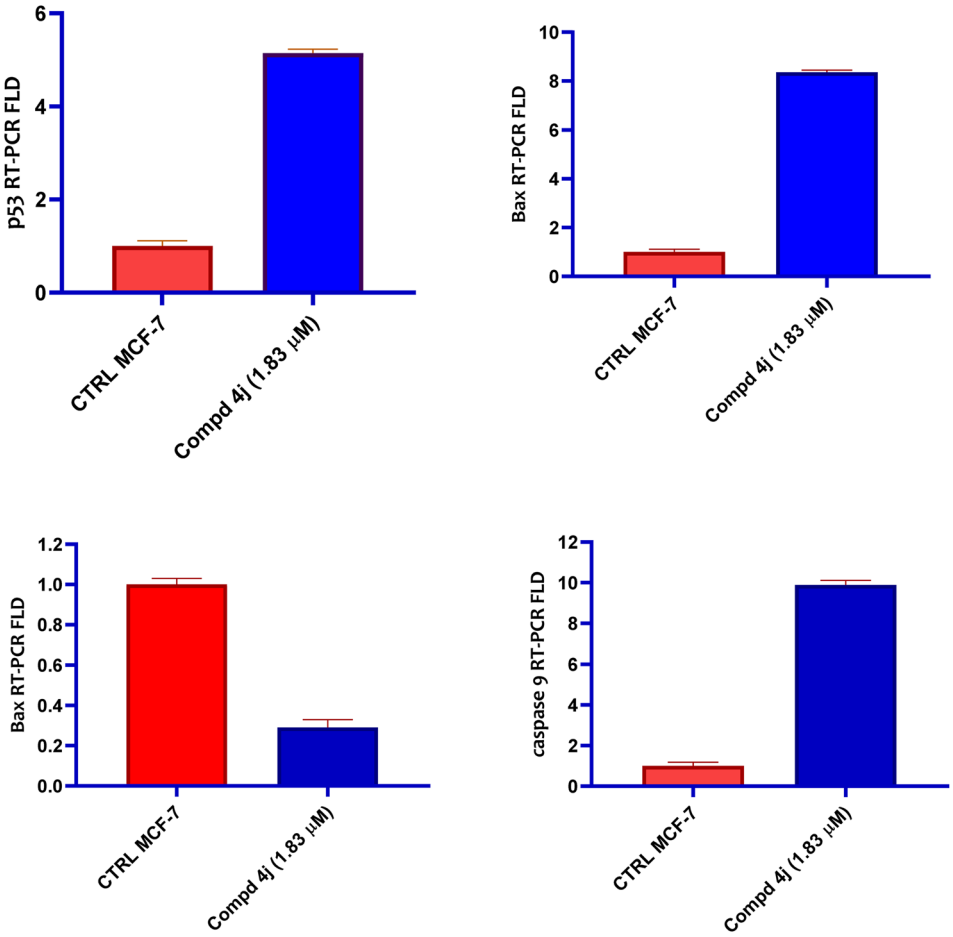

Fig. 4 *In vitro* qRT-PCR measurements of the expression levels of p53, Bax, Bcl-2 and caspase 9 in MCF-7 cells stimulated by the acrylamide–PABA analog **4j** relative to negative control cells.

PABA analog **4j**-induced cytotoxicity against the MCF-7 cancer cell line.

2.2.5. Acrylamide–PABA analog 4j promoted cellular cycle arrest at the G2\M phase in MCF-7 cells. In cancer mass development, the disruption of the cell cycle can be an important event. Cellular cycle progression has two primary checkpoints: G1/S before DNA replication and G2/M before mitosis.[33] A p53-responsive gene such as $p21^{wafi}$ regulates the G1/S checkpoint and mediates cell cycle arrest.[34] Since the cytotoxic activity of the synthesized analogs against MCF-7 cells was induced by the enhanced apoptotic levels, we examined whether these analogs further induced cell cycle arrest. MCF-7 cells were treated with the most active acrylamide–PABA **4j** member for 48 h, dyed with PI and then subjected to flow cytometric analysis in order examine the distribution of the cellular cycle. As can been seen in Fig. 5, the cellular distribution at each stage is depicted in the histogram of the cellular cycle caused by the acrylamide–PABA hybrid **4j**. It showed that compound **4j** significantly promoted cellular cycle arrest mainly at the G2/M phase (34.18%) compared with the untreated control group (9.41%). On the other hand, the analog **4j** significantly decreased the cellular population at both G1 phase (46.99%) and S phase (18.83%) with regard to the negative controls [(61.08%) and (29.51%)], respectively. Hence, the promotion of the cell cycle arrest at the G2/M phase is another mechanism that explains the cytotoxicity of the acrylamide–PABA hybrid **4j** against MCF-7 cells.

2.3. Molecular modelling study

Molecular docking studies were performed to elucidate the superior cytotoxicity and tubulin inhibitory activity of the PABA–acrylamide–CA-4 hybrids, **4a** and **4j**, compared to CA-4. Notably, CA-4, **4a**, and **4j** were found to be superimposed and optimally positioned within the colchicine binding site of tubulin (Fig. 6), with binding free energies of −6.2, −8.0, and −8.1 kcal mol^{-1}, respectively. Detailed analysis revealed that CA-4, **4a**, and **4j** (Fig. 7–9) established hydrogen bonding interactions with the key amino acid residue Cys241. Additionally, strong hydrophobic interactions with Gln247, Leu248, Ala250, Lys254, Leu255, Asn258, Lys352, and Ala316 were identified within the tubulin binding pocket.[35,36]

This exceptional tubulin-binding inhibitory activity may be attributed to the newly incorporated PABA fragment, which anchors within a hydrophobic pocket flanked by Lys352, Met259, and Asn258. Additionally, strong hydrogen bonding

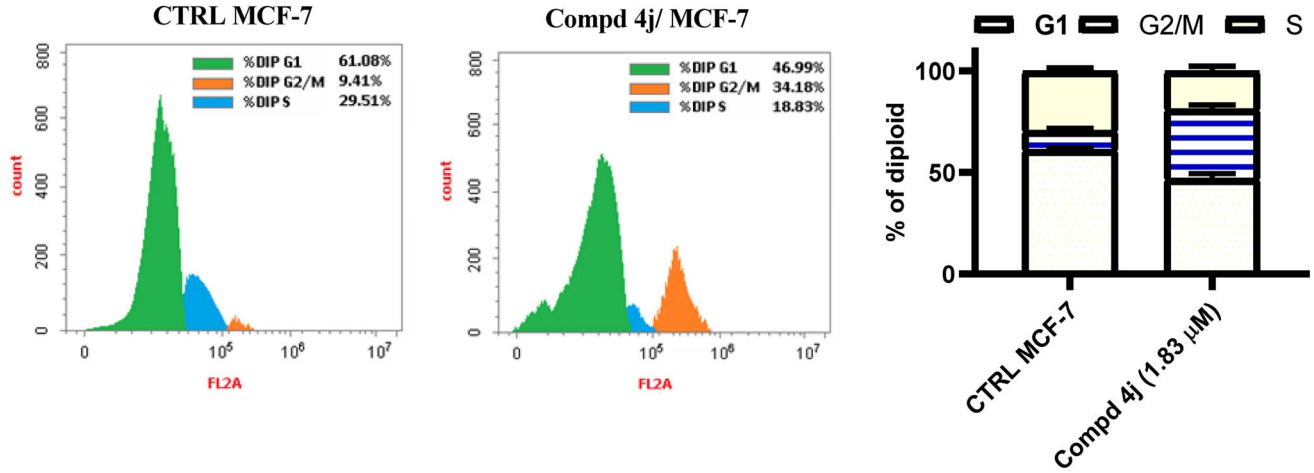

Fig. 5 Cellular cycle distribution of MCF-7 cells stimulated by acrylamide–PABA analogs **4j** relative to untreated controls.

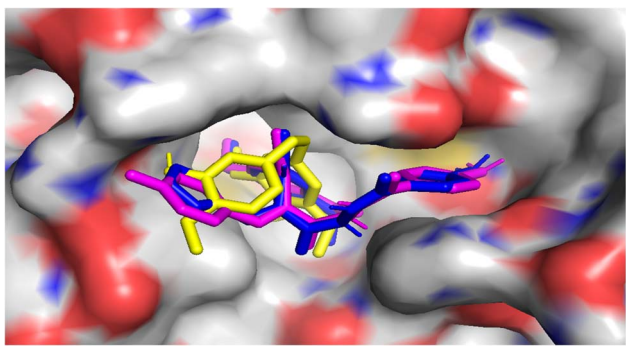

Fig. 6 Surface view representation of the superimposition of CA-4 (yellow), **4a** (magenta) and **4j** (blue) in the colchicine-binding pocket of tubulin.

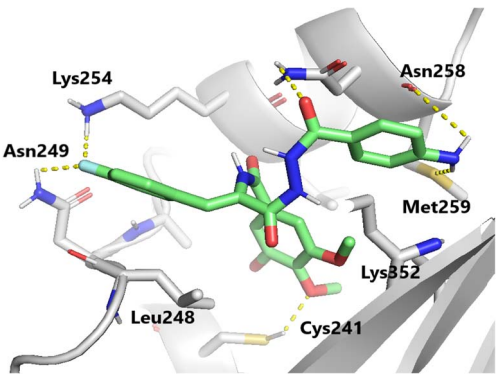

Fig. 8 Binding mode of compound **4a** in the colchicine-binding pocket of tubulin. Hydrogen bonds are shown using yellow dashed lines.

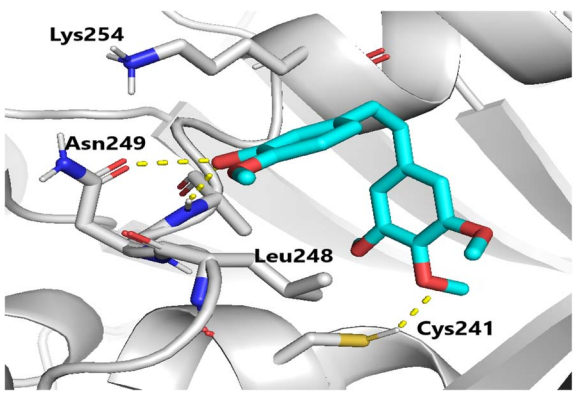

Fig. 7 Binding mode of CA-4 in the colchicine-binding pocket of tubulin. Hydrogen bonds are shown using yellow dashed lines.

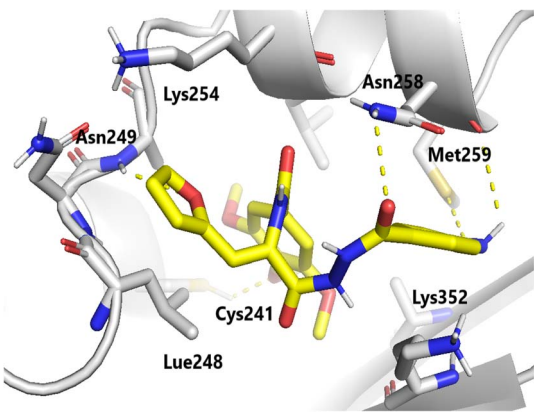

Fig. 9 Binding mode of compound **4j** in the colchicine-binding pocket of tubulin. Hydrogen bonds are shown using blue dashed lines.

interactions were observed with Asn258 and Met259, further stabilizing the complex. Moreover, the 4-F-phenyl fragment **4a** and the 2-furanyl group **4j** are positioned within a hydrophobic pocket bordered by Leu248, Asn249, and Lys254. Furthermore, the formation of additional hydrogen bonds with Asn249 and Lys254 contributes to the enhanced stability of these ligand–tubulin complexes. The docking results show that for the PABA–acrylamide–CA-4 hybrids, **4a** and **4j**, the cytotoxicity against MCF-7 may result from their ability to inhibit tubulin polymerization.

Table 2 Anticipated aqueous solubility and BBB penetration of the acrylamide–PABA compounds **4a–j**

Comp. no.	Aq. solubility level	BBB level
4a	2	4
4b	2	4
4c	2	4
4d	2	4
4e	2	4
4f	3	4
4g	2	4
4h	1	4
4i	2	4
4j	3	4

2.4. *In Silico* predictive ADME study for synthesized acrylamide–PABA 4a–j

The ADME descriptors tool in Discovery Studio was used to assess the in *s*ilico pharmacokinetic profiles of the synthesized PAPA–acrylamide derivatives **4a–j** (Table 2). Important pharmacokinetic factors were anticipated, such as the blood–brain barrier level (BBB level) and aqueous solubility level.[37,38] The BBB level value of 4 for all synthesized compounds indicated that they were unable to pass through the blood–brain barrier. This finding is beneficial since it may lessen the likelihood of adverse effects involving the central nervous system.

Furthermore, the compounds' expected degrees of aqueous solubility ranged from low to good. The most potent antiproliferative candidate in the series, compound **4j**, notably showed a good aqueous solubility profile (aq. sol. level: 3). This result is quite noteworthy and consistent with our study's main goal. The parent compound CA-4 is characterized by poor water solubility, which limits its bioavailability and therapeutic performance. In this study, we strategically designed acrylamide–PAPA derivatives by integrating PABA to enhance the polarity and overall solubility. The enhanced water solubility of compound **4j** serves as a strong indication that this design approach is effective, potentially overcoming one of the major pharmacokinetic limitations of CA-4.

3. Conclusions

The intricate molecular pathways governing β-tubulin-microtubule dynamics and apoptosis are two obvious targets for pharmacological interventions, given their significant significance in the formation and evolution of cancerous tumors. So, focusing on the inhibition of β-tubulin polymerization and apoptosis promotion is a desirable approach for successful cancer therapy. As an approach, a new series of acrylamide–PABA analogs **4a–j** have been constructed and tested for their ability to inhibit the MCF-7 breast cancer cell line. The acrylamide–PABA analog **4j** was found to have strong cytotoxic action *via* β-tubulin polymerization inhibition and activating apoptosis. The apoptotic effect of the most active analog was extensively investigated and showed a marked increase in p53 and Bax levels up to 5.14- and 8.36-fold, respectively, accompanied by down-regulation of Bcl-2 to 0.29-fold relative to the controls. Furthermore, the influence of compound **4j** on *c*aspase 9 was evaluated. It was found to enhance its level by 9.89-fold in comparison to the untreated controls. The effect of compound **4j** on the cell cycle was also examined. Results revealed that compound **4j** causes the MCF-7 cells to arrest at the G2/M phase compared to the untreated controls.

4. Experimental

4.1. Chemistry

4.1.1. General method for the synthesis of (*Z*)-*N*-(3-(2-(4-aminobenzoyl)hydrazineyl)-1-aryl-3-oxoprop-1-en-2-yl)-3,4,5-trimethoxybenzamides 4a–j. A mixture of 4-aminobenzohydrazide (0.0028 mol, 0.42 g) and appropriate ethyl 3-arylacrylate (0.0028 mol) in pure ethanol (20 mL) and glacial acetic acid (2 mL) was refluxed for 10–12 h. The reaction mixture was cooled and poured into ice-cold water once the reaction was finished. The acrylamide–PABA analogs **4a–j** were achieved by filtering and crystallizing the separated solid from the alcohol.

*4.1.1.1. (Z)-N-(3-(2-(4-Aminobenzoyl)hydrazineyl)-1-(4-fluorophenyl)-3-oxoprop-1-en-2-yl)-3,4,5-trimethoxybenzamide (**4a**).* Yield: 72%, m.p. 228–230 °C. ^{1}H-NMR (400 MHz, DMSO-d_6) δ: 10.03 (s, 1H, NH), 9.96 (s, 1H, NH), 9.94 (s, 1H, NH), 7.68 (d, J = 9.1 Hz, 2H), 7.65 (d, J = 3.2 Hz, 2H), 7.36 (s, 2H), 7.31 (s, 1H, olefinic CH), 7.25 (t, J = 8.9 Hz, 2H), 6.56 (d, J = 8.7 Hz, 2H), 5.70 (s, 2H, NH_2), 3.85 (s, 6H, $2OCH_3$), 3.74 (s, 3H, OCH_3). ^{13}C-NMR (101 MHz, DMSO) δ: 166.06, 165.87, 165.28, 161.24, 153.00, 152.56, 140.85, 132.14, 132.06, 131.12, 129.61, 129.44, 129.19, 129.01, 128.86, 119.59, 116.17, 113.01, 106.10, 60.57, 56.53. Analysis: Calc. for $C_{26}H_{25}FN_4O_6$ (508.51): C 61.41, H 4.96, N 11.02%, found: C 61.52, H 5.07, N 10.89%.

*4.1.1.2. (Z)-N-(3-(2-(4-Aminobenzoyl)hydrazineyl)-1-(4-chlorophenyl)-3-oxoprop-1-en-2-yl)-3,4,5-trimethoxybenzamide (**4b**).* Yield: 74%, m.p. 239–241 °C. ^{1}H-NMR (400 MHz, DMSO-d_6) δ: 10.07 (s, 1H, NH), 9.96 (s, 2H, NH_2), 7.68–7.64 (m, 2H), 7.64–7.60 (m, 2H), 7.57–7.52 (m, 2H), 7.36 (s, 2H), 7.27 (s, 1H, olefinic CH), 6.59–6.55 (m, 2H), 5.71 (s, 2H, NH_2), 3.86 (s, 6H, $2OCH_3$), 3.74 (s, 3H s, 3H, OCH_3). ^{13}C-NMR (101 MHz, DMSO) δ: 166.90, 166.07, 165.21, 153.01, 151.98, 140.89, 133.52, 131.55, 130.36, 129.62, 129.12, 128.87, 128.58, 120.41, 119.56, 113.02, 106.11, 60.57, 56.54. Analysis: Calc. for $C_{26}H_{25}ClN_4O_6$ (524.96): C 59.49, H 4.80, N 10.67%, found: C 59.38, H 4.85, N 10.78%.

*4.1.1.3. (Z)-N-(3-(2-(4-Aminobenzoyl)hydrazineyl)-1-(4-nitrophenyl)-3-oxoprop-1-en-2-yl)-3,4,5-trimethoxybenzamide (**4c**).* Yield: 76%, m.p. 243–245 °C. ^{1}H-NMR (400 MHz, DMSO-d_6) δ: 10.12 (s, 2H, 2NH), 10.02 (s, 1H, NH), 8.25 (d, J = 8.8 Hz, 2H), 7.84 (d, J = 8.6 Hz, 2H), 7.66 (d, J = 8.3 Hz, 2H), 7.35 (s, 2H), 7.31 (s, 1H, olefinic CH), 6.57 (d, J = 8.6 Hz, 2H), 5.72 (s, 2H, NH_2), 3.85 (s, 6H, $2OCH_3$), 3.74 (s, 3H, OCH_3). ^{13}C-NMR (101 MHz, DMSO) δ: 166.89, 165.84, 164.99, 153.03, 151.98, 147.15, 141.62, 133.07, 130.74, 129.64, 128.87, 126.75, 124.18, 120.40, 119.47, 113.02, 106.18, 60.58, 56.56. Analysis: Calc. for $C_{26}H_{25}N_5O_8$ (535.51): C 58.32, H 4.71, N 13.08%, found: C 58.43, H 4.58, N 12.98%.

*4.1.1.4. (Z)-N-(3-(2-(4-Aminobenzoyl)hydrazineyl)-3-oxo-1-(p-tolyl)prop-1-en-2-yl)-3,4,5-trimethoxybenzamide (**4d**).* Yield: 68%,

m.p. 237–239 °C. ^{1}H-NMR (400 MHz, DMSO-d_6) δ: 9.97 (s, 2H, 2NH), 9.90 (s, 1H, NH), 7.66 (d, J = 8.2 Hz, 2H), 7.51 (d, J = 7.8 Hz, 2H), 7.38 (s, 2H), 7.29 (s, 1H, olefinic CH), 7.21 (d, J = 7.8 Hz, 2H), 6.57 (d, J = 8.3 Hz, 2H), 5.70 (s, 2H, NH_2), 3.86 (s, 6H, 2OCH_3), 3.74 (s, 3H, OCH_3), 2.30 (s, 3H, CH_3). ^{13}C-NMR (101 MHz, DMSO) δ: 166.09, 165.85, 165.42, 152.99, 152.55, 140.79, 139.08, 131.69, 130.38, 129.97, 129.66, 129.61, 129.33, 128.76, 119.60, 113.02, 106.08, 60.58, 56.53, 21.37. Analysis: Calc. for $C_{27}H_{28}N_4O_6$ (504.54): C 64.28, H 5.59, N 11.10%, found: C 64.44, H 5.71, N 11.01%.

*4.1.1.5. (Z)-N-(3-(2-(4-Aminobenzoyl)hydrazineyl)-1-(4-methoxyphenyl)-3-oxoprop-1-en-2-yl)-3,4,5-trimethoxybenzamide (**4e**).* Yield: 73%, m.p. 226–228 °C. ^{1}H-NMR (400 MHz, DMSO-d_6) δ: 10.01 (s, 1H, 2NH), 9.96 (s, 1H, 2NH), 9.87 (s, 1H, NH), 7.65 (d, J = 8.3 Hz, 2H), 7.58 (d, J = 8.4 Hz, 2H), 7.38 (s, 2H), 7.30 (s, 1H, olefinic CH), 6.96 (d, J = 8.4 Hz, 2H), 6.56 (d, J = 8.3 Hz, 2H), 5.69 (s, 2H, NH_2), 3.86 (s, 6H, 2OCH_3), 3.76 (s, 3H, OCH_3), 3.74 (s, 3H, OCH_3). ^{13}C-NMR (101 MHz, DMSO) δ: 166.08, 165.83, 165.50, 160.21, 152.99, 152.54, 140.77, 131.72, 130.43, 129.60, 129.39, 127.33, 126.95, 119.66, 114.57, 113.02, 106.09, 60.57, 56.53, 55.69. Analysis: Calc. for $C_{27}H_{28}N_4O_7$ (520.54): C 62.30, H 5.42, N 10.76%, found: C 62.47, H 5.28, N 10.61%.

*4.1.1.6. (Z)-N-(3-(2-(4-Aminobenzoyl)hydrazineyl)-1-(4-(dimethylamino)phenyl)-3-oxoprop-1-en-2-yl)-3,4,5-trimethoxybenzamide (**4f**).* Yield: 77%, m.p. 215–217 °C. ^{1}H-NMR (400 MHz, DMSO-d_6) δ: 9.89 (s, 1H, NH), 9.79 (s, 1HNH), 9.78 (s, 1H, NH), 7.65 (d, J = 8.3 Hz, 2H), 7.48 (d, J = 8.5 Hz, 2H), 7.41 (s, 2H), 7.30 (s, 1H, olefinic CH), 6.70 (d, J = 8.6 Hz, 2H), 6.56 (d, J = 8.2 Hz, 2H), 5.69 (s, 2H, NH_2), 3.87 (s, 6H, 2OCH_3), 3.75 (s, 3H, OCH_3), 2.93 (s, 6H, $N(CH_3)_2$). ^{13}C-NMR (101 MHz, DMSO) δ: 166.05, 165.72, 165.71, 152.49, 151.06, 140.66, 135.26, 131.68, 129.58, 127.52, 124.48, 121.77, 119.74, 113.00, 112.15, 106.08, 105.06, 60.57, 56.53, 40.15. Analysis: Calc. for $C_{28}H_{31}N_5O_6$ (533.59): C 63.03, H 5.86, N 13.13%, found: C 62.87, H 5.97, N 13.22%.

*4.1.1.7. (Z)-N-(3-(2-(4-Aminobenzoyl)hydrazineyl)-1-(3,4-dimethoxyphenyl)-3-oxoprop-1-en-2-yl)-3,4,5-trimethoxybenzamide (**4g**).* Yield: 71%, m.p. 211–213 °C. ^{1}H-NMR (400 MHz, DMSO-d_6) δ: 9.98 (d, J = 19.5 Hz, 2H), 9.84 (s, 1H), 7.68 (t, J = 4.7 Hz, 2H), 7.65 (s, 1H), 7.55 (d, J = 8.3 Hz, 1H), 7.34 (s, 1H, olefinic CH), 7.07 (d, J = 8.4 Hz, 1H), 7.00 (s, 2H), 6.57 (d, J = 8.4 Hz, 2H), 5.70 (s, 2H, NH_2), 3.84 (s, 3H, OCH_3), 3.82 (s, 3H, OCH_3), 3.67 (s, 3H, OCH_3), 3.63 (s, 6H, 2OCH_3). ^{13}C-NMR (101 MHz, DMSO) δ: 166.90, 165.92, 165.27, 153.04, 152.54, 151.98, 148.54, 138.51, 130.88, 129.91, 129.61, 128.87, 126.40, 121.94, 119.63, 113.05, 111.73, 111.22, 107.61, 60.52, 56.10, 56.08. Analysis: Calc. for $C_{28}H_{30}N_4O_8$ (550.57): C 61.08, H 5.49, N 10.18%, found: C 60.98, H 5.34, N 10.29%.

*4.1.1.8. (Z)-N-(3-(2-(4-Aminobenzoyl)hydrazineyl)-1-(3,5-dibromo-4-hydroxyphenyl)3-oxoprop-1-en-2-yl)-3,4,5-trimethoxybenzamide (**4h**).* Yield: 67%, 238–240 °C. ^{1}H-NMR (400 MHz, DMSO-d_6) δ: 10.14 (s, 1H, NH), 10.00 (d, J = 12.1 Hz, 1H, NH), 9.91 (d, J = 22.6 Hz, 1H, NH), 7.99 (s, 1H, OH), 7.84 (s, 2H, Ar–H), 7.64 (dd, J = 8.6, 2.6 Hz, 2H, Ar–H), 7.32 (s, 2H, Ar–H), 7.29 (d, J = 14.2 Hz, 1H, olefinic CH), 6.61–6.50 (m, 2H, Ar–H), 5.70 (s, 2H, NH_2), 3.86 (s, 6H, 2OCH_3), 3.73 (s, 3H, OCH_3). ^{13}C-NMR (101 MHz, DMSO) δ: 165.52, 164.41, 164.12, 152.56, 152.09, 145.18, 140.29, 135.22, 133.25, 132.92, 129.14, 128.73, 119.09, 117.14, 112.53, 111.75, 105.40, 60.15, 56.06. Analysis: Calc. for $C_{26}H_{24}Br_2N_4O_7$ (664.31): C 47.01, H 3.64, N 8.43%, found: C 46.86, H 3.76, N 8.59%.

*4.1.1.9. (Z)-N-(3-(2-(4-Aminobenzoyl)hydrazineyl)-3-oxo-1-(3,4,5-trimethoxyphenyl)prop-1-en-2-yl)-3,4,5-trimethoxybenzamide (**4i**).* Yield: 73%, m.p. 230–232 °C. ^{1}H NMR (400 MHz, DMSO-d_6) δ: 10.05 (s, 1H, NH), 9.98 (s, 1H, NH), 9.95 (s, 1H, NH), 7.80–7.66 (m, 2H), 7.45 (s, 2H), 7.39 (s, 1H, olefinic CH), 7.02 (s, 2H), 6.59 (d, J = 8.1 Hz, 2H), 5.72 (s, 2H), 3.86 (s, 9H, 3OCH_3), 3.75 (s, 3H, OCH_3), 3.67 (s, 6H, 2OCH_3). ^{13}C-NMR (101 MHz, DMSO) δ: 166.05, 165.83, 165.18, 153.07, 152.96, 152.57, 140.86, 138.61, 132.40, 131.13, 129.63, 129.29, 128.67, 119.63, 113.03, 107.67, 106.06, 60.64, 60.53, 56.55, 56.08. Analysis: Calc. for $C_{29}H_{32}N_4O_9$ (580.59): C 59.99, H 5.56, N 9.65%, found: C 60.11, H 5.72, N 9.52%.

*4.1.1.10. (Z)-N-(3-(2-(4-Aminobenzoyl)hydrazineyl)-1-(furan-2-yl)-3-oxoprop-1-en-2-yl)-3,4,5-trimethoxybenzamide (**4j**).* Yield: 75%, m.p. 219–221 °C. ^{1}H NMR (400 MHz, DMSO-d_6) δ: ^{1}H-NMR (400 MHz, DMSO-d_6) δ: 10.01 (s, 1H, NH), 9.96 (s, 1H, NH), 9.83 (s, 1H, NH), 7.85–7.76 (m, 1H), 7.65 (d, J = 8.2 Hz, 2H), 7.40 (s, 2H), 7.24 (s, 1H, olefinic CH), 6.76 (d, J = 3.5 Hz, 1H), 6.64–6.60 (m, 1H), 6.57 (d, J = 8.2 Hz, 2H), 5.71 (s, 2H, NH_2), 3.87 (s, 6H, 2OCH_3), 3.75 (s, 3H, OCH_3). ^{13}C-NMR (101 MHz, DMSO) δ: 166.06, 165.71, 164.68, 152.99, 152.56, 150.06, 145.17, 140.77, 129.61, 129.51, 126.80, 119.57, 118.65, 114.72, 113.02, 112.83, 106.09, 60.58, 56.53. Analysis: Calc. for $C_{24}H_{24}N_4O_7$ (480.48): C 60.00, H 5.03, N 11.66%, found: C 60.06, H 4.98, N 11.59%.

4.2. Biological study

The biological activity studies of the constructed acrylamide–PABA molecules **4a–j** were added in the ESI see Appendix A.†

Data availability

The authors confirm that the data supporting the findings of this study are available within the article and/or its ESI.†

Conflicts of interest

No potential conflict of interest was reported by the author(s).

Acknowledgements

The authors extend their appreciation to the Deanship of Scientific Research and Graduate Studies at King Khalid University for funding this work through the Large Research Project under grant number RGP2/63/46. The authors also extend their appreciation to Princess Nourah bint Abdulrahman University Researchers Supporting Project number (PNURSP2025R465), Princess Nourah bint Abdulrahman University, Riyadh, Saudi Arabia.

References

1 L. Thangavelu, E. Moglad, G. Gupta, S. V. Menon, A. Gaur, S. Sharma, M. Kaur, M. Chahar, G. V. Sivaprasad and

M. Deorari, GAS5 lncRNA: A biomarker and therapeutic target in breast cancer, *Pathol., Res. Pract.*, 2024, **260**, 155424.
2 S. El Rhabori, M. Alaqarbeh, Y. El Allouche, L. Naanaai, A. El Aissouq, M. Bouachrine, S. Chtita and F. Khalil, Exploring innovative strategies for identifying anti-breast cancer compounds by integrating 2D/3D-QSAR, molecular docking analyses, ADMET predictions, molecular dynamics simulations, and MM-PBSA approaches, *J. Mol. Struct.*, 2025, **1320**, 139500.
3 World Health Organization. *Breast Cancer*. Retrieved from **https://www.who.int/news-room/fact-sheets/detail/breast**, (2024, March 13).
4 R. L. Siegel, A. N. Giaquinto and A. Jemal, Cancer statistics, 2024, *Ca-Cancer J. Clin.*, 2024, **74**, 12–49.
5 J. Kim, A. Harper, V. McCormack, H. Sung, N. Houssami, E. Morgan, M. Mutebi, G. Garvey, I. Soerjomataram and M. M. Fidler-Benaoudia, Global patterns and trends in breast cancer incidence and mortality across 185 countries, *Nat. Med.*, 2025, **31**, 1154–1162.
6 S. Łukasiewicz, M. Czeczelewski, A. Forma, J. Baj, R. Sitarz and A. Stanisławek, Breast Cancer—Epidemiology, Risk Factors, Classification, Prognostic Markers, and Current Treatment Strategies—An Updated Review, *Cancers*, 2021, **13**, 4287.
7 R. Colomer, B. González-Farré, A. I. Ballesteros, V. Peg, B. Bermejo, B. Pérez-Mies, S. de la Cruz, F. Rojo, S. Pernas and J. Palacios, Biomarkers in breast cancer 2024: an updated consensus statement by the Spanish Society of Medical Oncology and the Spanish Society of Pathology, *Clin. Transl. Oncol.*, 2024, **26**, 2935–2951.
8 M. S. A. Tantry and K. Santhakumar, Insights on the Role of α- and β-Tubulin Isotypes in Early Brain Development, *Mol. Neurobiol.*, 2023, **60**, 3803–3823.
9 H. M. A. El-Lateef, R. M. Saleem, M. A. Bazuhair, A. H. A. Maghrabi, E. H. K. Ali, I. Zaki and R. E. Masoud, Design, synthesis and tubulin polymerization inhibition activity of newly synthesized hydrazone-linked to combretastatin analogues as potential anticancer agents, *J. Mol. Struct.*, 2023, **1292**, 136190.
10 W. Zhao, R. Shen, H.-M. Li, J.-J. Zhong and Y.-J. Tang, Podophyllotoxin derivatives-tubulin complex reveals a potential binding site of tubulin polymerization inhibitors in α-tubulin adjacent to colchicine site, *Int. J. Biol. Macromol.*, 2024, **276**, 133678.
11 M. Hawash, Recent Advances of Tubulin Inhibitors Targeting the Colchicine Binding Site for Cancer Therapy, *Biomolecules*, 2022, **12**, 1843.
12 S. Deng, R. I. Krutilina, K. L. Hartman, H. Chen, D. N. Parke, R. Wang, F. Mahmud, D. Ma, P. B. Lukka, B. Meibohm, T. N. Seagroves, D. D. Miller and W. Li, Colchicine-Binding Site Agent CH-2-77 as a Potent Tubulin Inhibitor Suppressing Triple-Negative Breast Cancer, *Mol. Cancer Ther.*, 2022, **21**, 1103–1114.
13 E. Fayad, S. A. Altalhi, M. M. Abualnaja, A. H. Alrohaimi, F. G. Elsaid, A. H. Abu Almaaty, R. M. Saleem, M. A. Bazuhair, A. H. Ahmed Maghrabi, B. Y. Beshay and I. Zaki, Novel Acrylate-Based Derivatives: Design, Synthesis, Antiproliferative Screening, and Docking Study as Potential Combretastatin Analogues, *ACS Omega*, 2023, **8**, 38394–38405.
14 K. O. Mohamed, I. Zaki, I. M. El-Deen and M. K. Abdelhameid, A new class of diamide scaffold: Design, synthesis and biological evaluation as potent antimitotic agents, tubulin polymerization inhibition and apoptosis inducing activity studies, *Bioorg. Chem.*, 2019, **84**, 399–409.
15 N. E. A. A. El-Sattar, S. E. S. A. El-Hddad, M. M. Ghobashy, A. A. Zaher and K. El-Adl, Nanogel-mediated drug delivery system for anticancer agent: pH stimuli responsive poly(ethylene glycol/acrylic acid) nanogel prepared by gamma irradiation, *Bioorg. Chem.*, 2022, **127**, 105972.
16 D. S. Alshaya, R. M. Tawakul, I. Zaki, A. H. A. Almaaty, E. Fayad and Y. M. Abd El-Aziz, Design, synthesis and antiproliferative screening of newly synthesized acrylate derivatives as potential anticancer agents, *RSC Adv.*, 2023, **13**, 23538–23546.
17 M. Gao, D. Zhang, Q. Jin, C. Jiang, C. Wang, J. Li, F. Peng, D. Huang, J. Zhang and S. Song, Combretastatin-A4 phosphate improves the distribution and antitumor efficacy of albumin-bound paclitaxel in W256 breast carcinoma model, *Oncotarget*, 2016, **7**, 58133.
18 P. Nathan, M. Zweifel, A. R. Padhani, D.-M. Koh, M. Ng, D. J. Collins, A. Harris, C. Carden, J. Smythe, N. Fisher, N. J. Taylor, J. J. Stirling, S.-P. Lu, M. O. Leach, G. J. S. Rustin and I. Judson, Phase I Trial of Combretastatin A4 Phosphate (CA4P) in Combination with Bevacizumab in Patients with Advanced Cancer, *Clin. Cancer Res.*, 2012, **18**, 3428–3439.
19 H. Zhang, M. Li, X. Zhou, L. Tang, G. Chen and Y. Zhang, Design, synthesis of combretastatin A-4 piperazine derivatives as potential antitumor agents by inhibiting tubulin polymerization and inducing autophagy in HCT116 cells, *Eur. J. Med. Chem.*, 2024, **272**, 116497.
20 M.-Y. Song, Q.-R. He, Y.-L. Wang, H.-R. Wang, T.-C. Jiang, J.-J. Tang and J.-M. Gao, Exploring Diverse-Ring Analogues on Combretastatin A4 (CA-4) Olefin as Microtubule-Targeting Agents, *Int. J. Mol. Sci.*, 2020, **21**, 1817.
21 D.-J. Fu, J.-F. Liu, R.-H. Zhao, J.-H. Li, S.-Y. Zhang and Y.-B. Zhang, Design and Antiproliferative Evaluation of Novel Sulfanilamide Derivatives as Potential Tubulin Polymerization Inhibitors, *Molecules*, 2017, **22**, 1470.
22 H. Rajak, P. Kumar, P. Parmar, B. S. Thakur, R. Veerasamy, P. C. Sharma, A. K. Sharma, A. K. Gupta and J. S. Dangi, Appraisal of GABA and PABA as linker: Design and synthesis of novel benzamide based histone deacetylase inhibitors, *Eur. J. Med. Chem.*, 2012, **53**, 390–397.
23 L. V. Ramachandran, V. B. Nair, S. K. C. SunilKumar and A. C. Edoly, Design synthesis and *in vitro* anticancer activity of novel imidazolyl benzoic acid derivatives, *Chem. Lett.*, 2025, **6**, 135–141.
24 B. Sapijanskaitė-Banevič, V. Palskys, R. Vaickelionienė, J. Šiugždaitė, P. Kavaliauskas, B. Grybaitė and V. Mickevičius, Synthesis and Antibacterial Activity of New

Azole, Diazole and Triazole Derivatives Based on p-Aminobenzoic Acid, *Molecules*, 2021, **26**, 2597.

25 S. N. A. Bukhari, M. Y. Zakaria, M. U. Munir, N. Ahmad, M. A. Elsherif, R. E. Badr, A. K. Hassan, A. H. A. Almaaty and I. Zaki, Design, Synthesis, *In Vitro* Biological Activity Evaluation and Stabilized Nanostructured Lipid Carrier Formulation of Newly Synthesized Schiff Bases-Based TMP Moieties, *Pharmaceuticals*, 2022, **15**, 679.

26 X. Deng, X. Deng, W. Ning, L. Xin, Q. Li, Z. Hu, B. Xie, K. Liang, C. Min, C. Dong, J. Huang and H.-B. Zhou, Identification of Novel Dual-Target Estrogen Receptor α Degraders with Tubulin Inhibitory Activity for the Treatment of Endocrine-Resistant Breast Cancer, *J. Med. Chem.*, 2023, **66**, 11094–11117.

27 T. Al-Warhi, M. Abualnaja, O. A. Abu Ali, F. Althobaiti, F. Alharthi, F. G. Elsaid, A. A. Shati, E. Fayad, D. Elghareeb, A. H. Abu Almaaty and I. Zaki, Synthesis and Biological Activity Screening of Newly Synthesized Trimethoxyphenyl-Based Analogues as Potential Anticancer Agents, *Molecules*, 2022, **27**, 4621.

28 N. El Omari, S. Bakrim, A. Khalid, A. N. Abdalla, W. H. Almalki, L.-H. Lee, C. Ardianto, L. C. Ming and A. Bouyahya, Molecular mechanisms underlying the clinical efficacy of panobinostat involve Stochasticity of epigenetic signaling, sensitization to anticancer drugs, and induction of cellular cell death related to cellular stresses, *Biomed. Pharmacother.*, 2023, **164**, 114886.

29 P. Singh and B. Lim, Targeting Apoptosis in Cancer, *Curr. Oncol. Rep.*, 2022, **24**, 273–284.

30 T. N. Shenoy and A. A. Abdul Salam, Therapeutic potential of dietary bioactive compounds against anti-apoptotic Bcl-2 proteins in breast cancer, *Crit. Rev. Food Sci. Nutr.*, 2024, 1–26.

31 A. Kooti, H. Abuei, A. Jaafari, S. Taki, J. Saberzadeh and A. Farhadi, Activating transcription factor 3 mediates apoptosis and cell cycle arrest in TP53-mutated anaplastic thyroid cancer cells, *Thyroid Res.*, 2024, **17**, 12.

32 C. Peng, Y. Wang, Y. Guo, J. Li, F. Liu, Y. Fu, Y. Yu, C. Zhang, J. Fu and F. Han, A literature review on signaling pathways of cervical cancer cell death-apoptosis induced by Traditional Chinese Medicine, *J. Ethnopharmacol.*, 2024, **334**, 118491.

33 H. K. Matthews, C. Bertoli and R. A. M. de Bruin, Cell cycle control in cancer, *Nat. Rev. Mol. Cell Biol.*, 2022, **23**, 74–88.

34 Z. E. Winters, R. D. Leek, M. J. Bradburn, C. J. Norbury and A. L. Harris, Cytoplasmic p21WAF1/CIP1expression is correlated with HER-2/neu in breast cancer and is an independent predictor of prognosis, *Breast Cancer Res.*, 2003, **5**, R242.

35 W. Li, S. Honghao, X. Shengtao, Z. Zheying and J. Xu, Tubulin Inhibitors Targeting the Colchicine Binding Site: A Perspective of Privileged Structures, *Future Med. Chem.*, 2017, **9**, 1765–1794.

36 Y.-T. Duan, R.-J. Man, D.-J. Tang, Y.-F. Yao, X.-X. Tao, C. Yu, X.-Y. Liang, J. A. Makawana, M.-J. Zou, Z.-C. Wang and H.-L. Zhu, Design, Synthesis and Antitumor Activity of Novel link-bridge and B-Ring Modified Combretastatin A-4 (CA-4) Analogues as Potent Antitubulin Agents, *Sci. Rep.*, 2016, **6**, 25387.

37 N. Ryad, A. A. Elmaaty, S. Selim, M. S. Almuhayawi, S. K. Al Jaouni, M. S. Abdel-Aziz, A. S. Alqahtani, I. Zaki and L. M. A. Ghany, Design and synthesis of novel 2-(2-(4-bromophenyl) quinolin-4-yl)-1, 3, 4-oxadiazole derivatives as anticancer and antimicrobial candidates: *in vitro* and *in silico* studies, *RSC Adv.*, 2024, **14**, 34005–34026.

38 D. N. Binjawhar, F. A. Al-Salmi, O. A. A. Ali, M. A. Alghamdi, E. Fayad, R. M. Saleem, I. Zaki and N. Farouk, Design, synthesis and cytotoxic activity of molecular hybrids based on quinolin-8-yloxy and cinnamide hybrids and their apoptosis inducing property, *RSC Adv.*, 2024, **14**, 11443–11451.